



**Quantum confinement in optically active ultrathin (Cd,Mn)Te/(Cd,Mg)Te core/shell nanowires**Jakub Płachta <sup>1</sup>, Michał Zieliński,<sup>2</sup> Tomasz Kazimierczuk,<sup>3</sup> Piotr Kossacki,<sup>3</sup> and Piotr Wojnar <sup>1</sup><sup>1</sup>*Institute of Physics, Polish Academy of Sciences, Aleja Lotników 32/46, PL-02-668 Warsaw, Poland*<sup>2</sup>*Institute of Physics, Faculty of Physics, Astronomy and Informatics, Nicolaus Copernicus University, ul Grudziądzka 5, PL-87-100 Toruń, Poland*<sup>3</sup>*Institute of Experimental Physics, Faculty of Physics, University of Warsaw, ul. Pasteura 5, PL-02-093 Warsaw, Poland*

(Received 11 December 2022; revised 13 February 2023; accepted 14 February 2023; published 28 February 2023)

The fabrication of ultrathin (Cd,Mn)Te nanowires with diameters reaching values below 10 nm is reported. The thinning procedure relies on a thermally induced reverse reaction process applied to (Cd,Mn)Te nanowires grown using the vapor-liquid-solid method. The impact of quantum confinement is manifested by a distinct blueshift of the excitonic emission from individual nanowires. Cathodoluminescence mapping reveals that the optical emission originates from relatively short nanowire segments, which is explained in terms of exciton localization on irregularities of nanowire core diameter. Magneto-optical study performed on several individual nanowires reveals a change from light hole to heavy hole character of the excitonic emission depending on the emission energy, i.e., on the size of the emitting object. The results are interpreted in terms of the influence of axial and radial quantum confinement on excitons in ultrathin nanowires.

DOI: [10.1103/PhysRevB.107.075305](https://doi.org/10.1103/PhysRevB.107.075305)**I. INTRODUCTION**

Quantum confinement in semiconductor heterostructures has attracted research interest for decades [1]. Strikingly, between well-studied two-dimensional and zero-dimensional systems lays an underexplored region of one-dimensional quantum wires (QWRs). While the electrostatically or lithographically defined QWRs, dedicated to quantum transport measurements, are widely available, similar structures for optical experiments are scarce. On the other hand, the vapor-liquid-solid (VLS) growth mechanism has been frequently used to fabricate semiconductor wires with diameters of the order of tens to hundreds of nanometers, known as nanowires (NWs) [2,3]. This method makes it possible to control nearly every aspect of their morphology and yields a high amount of structures that usually exhibit high crystalline quality. This, in turn, allows for fine-tuning electronic and light emission properties in such objects, making them a suitable subject for optical experiments. However, using the VLS-growth mechanism to achieve arbitrarily low NW diameter still poses a challenge. Typical NWs grown by this method have diameters far too large for the observation of the radial quantum confinement in most of the semiconductors having intermediate band gaps.

Controlled synthesis of VLS-grown QWRs could allow many interesting applications on top of existing NW-based technologies. One-dimensional confinement of electrons results in several exciting properties not present in the three-dimensional bulklike NWs. In particular, structures with a theoretically infinite density of states at the band edge represent attractive building blocks for the construction of lasers [4]. The small diameter of QWR allows for more efficient manipulation of strain induced by the deposition of radial shells. Strain, in turn, can be used to control the energy landscape in the valence band, which defines the polarization of

the emitted light. In a recent paper [5], a strong, temperature robust, linear polarization of the optical emission from (In,Ga)N/GaN wurtzite horizontal QWRs was reported. The polarization anisotropy is demonstrated to stem solely from the one-dimensional electron confinement present in these structures.

Moreover, the increase of electron-hole wave-function overlap and the ability to tune the emission energy solely via radial quantum confinement within a QWR are certainly promising for the development of cheaper and more efficient light sources. One-dimensional electron confinement results additionally in an enhancement of thermoelectric properties in GaAs/(Al,Ga)As QWRs [6] and is responsible for a significant increase of the electron spin lifetime which has great potential in view of long range transport of coherent spin information [7].

The majority of available works about optical properties of QWRs describe their fabrication either via epitaxial growth on lithographically defined templates [5,8] or solution-based methods [9–11]. In the other approaches, QWRs are demonstrated to form spontaneously at the faceted edges of Ga(As,P)/Ga(As,P) NW core/shell interface [12] and at one-dimensional extended crystal phase defects present within GaN NWs [13].

The growth of QWRs by using the VLS mechanism has been proposed by Loitsch *et al.* [14]. In that case, GaAs NWs grown using the VLS method are subject to *in situ* thinning via a thermally induced reverse reaction process. The resulting QWRs have diameters in the range 7–25 nm. Correlated optical and structural study reveals a significant impact of the radial quantum confinement on the optical emission energy. An improvement to this technique is presented in Ref. [15] where a similar process is tightly controlled by quadruple mass spectrometry, measuring Ga flux desorbed from the

GaN sample. This allows the reduction of NW diameters down to 6 nm, starting from more than 20 nm, and results in observation of excitonic emission up to the room temperature. In another, similar approach to GaAs NWs thinning [16], photoluminescence excitation spectroscopy combined with transmission electron microscopy are used to determine effective masses in subbands formed by the one-dimensional confinement. The NW-thinning procedure has also been applied for InAs NWs [17], where the one-dimensional character of the confinement has been confirmed by electron transport measurements. Finally, a detailed study of thermal decomposition of GaAs NWs has been performed resulting in NWs with diameters reaching values less than 10 nm [18].

In this work, the thermally induced reverse reaction process, previously applied only for III-V semiconductor NWs [14–16], has been adapted for II-VI semiconductor NWs containing a small molar fraction of magnetic Mn ions. As a result, ultrathin (Cd,Mn)Te NWs reaching below 10 nm in diameter are obtained. The advantage of the use of Mn-containing II-VI semiconductors is the opportunity to determine the light hole (LH)–heavy hole (HH) splitting values within the studied nanostructures [19,20]. Importantly, it is found that not only the LH–HH splitting but also the character of the excitonic emission depends on the emission energy. Simultaneously, the cathodoluminescence study reveals that the excitonic emission originates only from segments of NW cores, whereas shorter emitters tend to emit light at higher energy. These results are explained in terms of exciton localization at irregularities of NW-core diameters and the resulting influence of axial and radial quantum confinement.

## II. GROWTH

CdTe/(Cd,Mg)Te core/shell NWs are grown in molecular beam epitaxy setup by employing the VLS growth mechanism assisted with gold catalysts. Details of the growth procedure have been described previously [21]. Only the most important points are mentioned here. The NW growth starts with short ZnTe segments, which are followed by the proper straight (Cd,Mn)Te NWs grown at 350 °C. Mn concentration is of the order of 1%, which does not impact the NW growth itself but is crucial for the magneto-optical experiments. In order to reduce (Cd,Mn)Te NW-core diameters an annealing step is introduced before the shell deposition. Since the initial ZnTe base is characterized by a higher desorption temperature, it is not affected by the annealing process. The samples with ultrathin NWs were prepared along with a reference, grown in identical conditions without the annealing step, to directly compare the impact of the NW-core diameters on the optical emission spectrum. In the final stage the NWs are coated with a 25-nm-thick (Cd,Mg)Te shell containing Mg concentration of 35%, ensuring the passivation of surface states and the activation of the optical emission. High Mg content was chosen, so the potential well is deep enough to observe emission from excited states.

For the annealing process, two important parameters have to be found: the annealing temperature and the annealing time, both very demanding in terms of control. Multiple means were taken to ensure repeatability, among them a careful choice

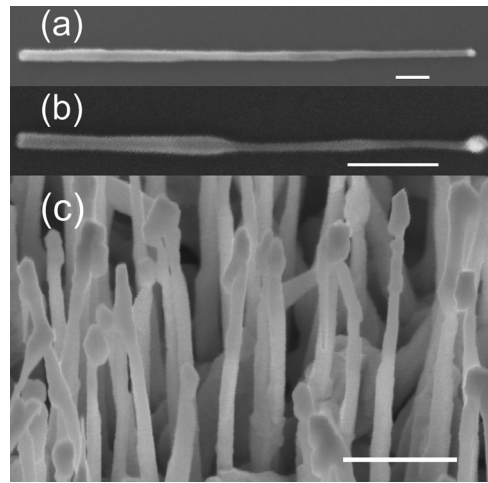


FIG. 1. Scanning electron microscope study of bare (Cd,Mn)Te and (Cd,Mn)Te/(Cd,Mg)Te core/shell NWs. (a) Single, detached (Cd,Mn)Te NW which was not subject to the annealing procedure. (b) (Cd,Mn)Te NW annealed at 395 °C for 30 min. Scale bars in (a) and (b) are 100 nm (note different scales). (c) Annealed (Cd,Mn)Te NWs with (Cd,Mg)Te shells. Image taken at 45 ° stage tilt. Scale bar is 500 nm. Probe current for all images is 150 nA and the electron acceleration voltage is 5 kV.

of the molybdenum template on which the samples were mounted during the growth, as well as a definition of the external dimensions of the samples. The progress of annealing was carefully inspected *in situ* by the means of reflection of high energy electron diffraction (RHEED), where the intensity of the pattern was tracked. During the annealing, the RHEED pattern slowly dimmed, up to a point where it vanished completely when all material was desorbed from the substrate. The optimal process conditions, which led to a controllable desorption, were found to be 30 min at 45 °C above the growth temperature of (Cd,Mn)Te NWs. The entire annealing procedure has been performed at Te flux corresponding to the beam equivalent pressure of  $6.3 \times 10^{-7}$  torr.

A typical (Cd,Mn)Te NW, which was not subject to the thermal treatment, has a tapered shape with a diameter ranging 30–50 nm, Fig. 1(a). After annealing in the optimal conditions, the NWs are significantly reduced, reaching diameters well below 10 nm in the thinnest place. Moreover, an inhomogeneity of NW diameter occurs in several NWs, as exemplified in Fig. 1(b). After coating the NWs with a (Cd,Mg)Te shell, the overall NW diameters increase up to 50–70 nm, Fig. 1(c). We note, however, that the inhomogeneity of NW diameters is still observable. The variation of NW-core diameter and (Cd,Mg)Te shell thickness results in different strain conditions along the NW axis, which may significantly affect the properties of charge carriers within this structure.

## III. PHOTOLUMINESCENCE

An expected indication of NW-diameter reduction as a result of the annealing process is a blueshift of the optical emission induced by the quantum size effect. The optical emission from (Cd,Mn)Te/(Cd,Mg)Te core/shell NWs in which the NW cores were subject to the thinning procedure

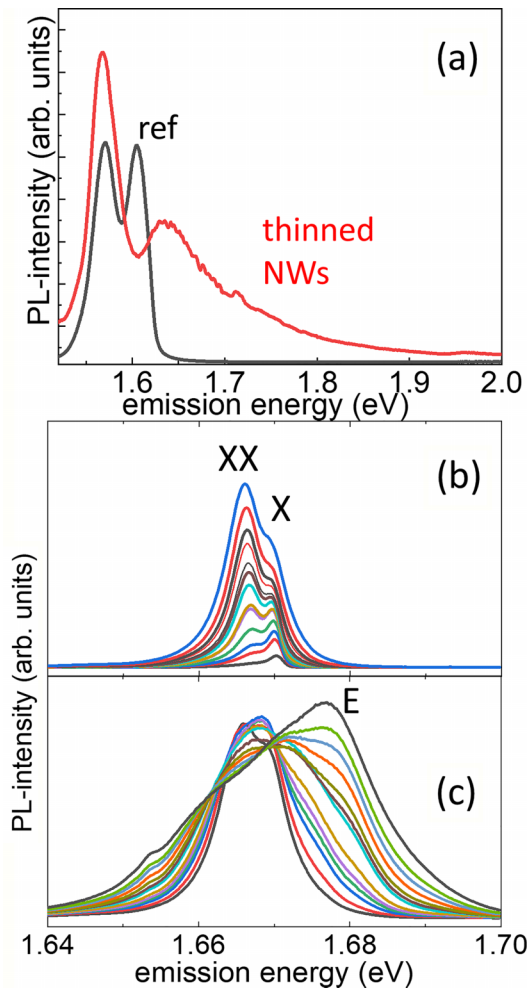


FIG. 2. (a) Photoluminescence from ensembles of (Cd,Mn)Te/(Cd,Mg)Te core/shell NWs. Thermally thinned NWs (red) compared to a reference sample (black). Photoluminescence from a single NW as a function of excitation fluence. (b) 1–20  $\mu\text{W}$ . (c) 30–500  $\mu\text{W}$ . Single exciton  $X$ , biexciton,  $XX$ , and excited state  $E$ ; related emissions are identified. Temperature of the measurements is 7 K, excitation wavelength is 532 nm (2.33 eV).

(red line) is compared to reference NWs grown in identical conditions but without the annealing step (black line) in Fig. 2(a). Most importantly, the peak of the excitonic emission, which appears at 1.61 eV in the reference sample, is significantly broadened and blueshifted by around 0.4 eV in the annealed sample. The broadening originates from the aforementioned inhomogeneous nature of the annealing process, resulting in the presence of NWs with different diameters within the NW ensemble. In both spectra, the defect related emission at around 1.55 eV and the shell-related emission at 2.32 eV (not shown) experience no shift between reference and annealed sample. This is expected, since the properties of these two emissions should not depend on the presence of the quantum confinement.

In the next step, the optical emission from individual NWs is studied in a microphotoluminescence setup. For these measurements, the NWs are removed from the original substrate and dispersed on a piece of clean silicon. The excitation

spot size is reduced down to 3  $\mu\text{m}$  and the laser beam is always perpendicular to the sample plane on which the NW lie flat.

It is found that the emission lines coming from individual thinned NWs in low excitation power have a spectral width of the order of a few meV, and their emission energy varies from 1.62 eV up to 1.80 eV, depending on a particular NW. This corresponds well to the observed broadening of the optical emission spectra from the NW ensemble, red curve in Fig. 2(a). In Fig. 2(b), a representative emission from a single NW is presented. At a low excitation power, only one emission line at 1.679 eV is present, while with the increase of excitation power, a second one emerges in a lower energy. The intensity of the high energy line increases linearly while that of the low energy line increases superlinearly with excitation power increase. This observation leads us to attribute them to exciton and biexciton emission, respectively. The latter complex is usually associated with low-dimensional objects where the quantum size effect plays an important role, such as in zero-dimensional quantum dots [22,23], and is not expected to appear in thick, bulklike NWs. Finally, Fig. 2(c) presents the emergence of additional emission lines in an even higher excitation power regime, related to an emission from excited states. Those emission lines are linearly polarized in the same direction as the excitonic and biexcitonic emission. Therefore, wurtzite CdTe segments can be excluded as their origin, since in wurtzite structure,  $B$  excitons are expected to be polarized perpendicularly to  $A$  excitons [24]. Most importantly, the presence of multiexcitonic emission in the optical spectrum from individual NWs confirms the low dimensional confinement of excitons within these structures.

#### IV. CATHODOLUMINESCENCE

To investigate the spatial positions and sizes of the emitting objects, a large set of single NWs was analyzed using low-temperature cathodoluminescence. In the first step, the cathodoluminescence (CL) spectrum from individual NWs was measured, usually consisting of one emission line, located between 1.62 and 1.80 eV, with a spectral width of a few meV. Then, monochromatic CL-maps with the energy corresponding to the maximum of the signal were collected and superimposed on the scanning electron microscope images of the studied NWs.

CL maps from two NWs emitting at two significantly different energies, 1.78 and 1.65 eV, are presented in Figs. 3(a) and 3(b), respectively. First of all, it is demonstrated that the studied emissions come, indeed, from the NWs and not from any other residual (Cd,Mn)Te deposits. Moreover, the analysis of the data reveals that the optical emission does not originate from entire NW cores but from segments, whereas the length of the emitting object may vary significantly depending on the particular NW. A general tendency is found that the shorter the emitting NW segment the higher the emission energy. However, the direct insight into the exact sizes of the emitters is overwhelmed by the carrier diffusion length along the NW axis [25]. The corresponding CL-intensity profiles along the NW axes are presented in Figs. 3(a') and 3(b'), respectively. The carrier diffusion effects are manifested as the monoexponential increase and decrease of the CL intensity, marked by the red lines. The carrier diffusion length typically



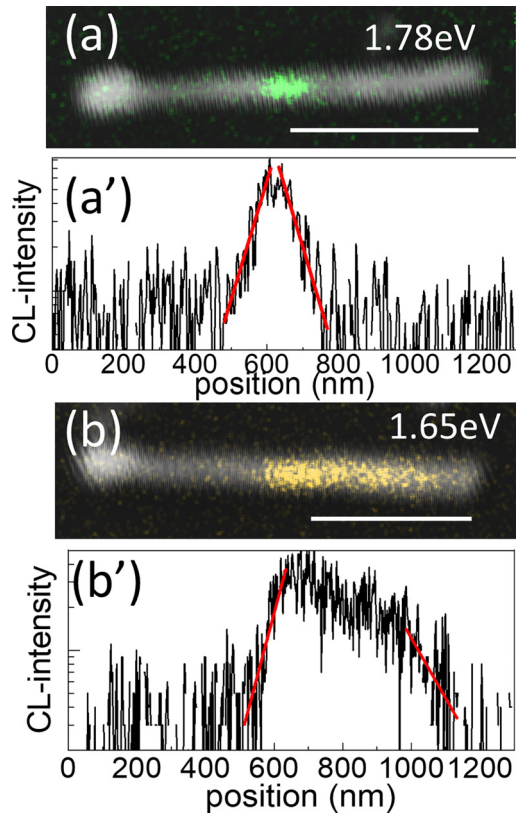


FIG. 3. Cathodoluminescence (CL) from two different thermally thinned (Cd,Mn)Te/(Cd,Mg)Te core/shell NWs emitting at 1.78 eV (a) and 1.65 eV (b); the corresponding CL-intensity profiles along the NW axis are plotted in logarithmic scale in (a') and (b'), respectively. Red lines represent fits with monoexponential growth/decay from which the carrier diffusion length is determined. Temperature of the measurements is 7 K, electron acceleration voltage is 15 kV, and the probe current is 150 nA.

amounts to several tens of nanometers. For instance, in the case of Fig. 3(a'), the carrier diffusion lengths are estimated to be 120 and 130 nm, which is significantly larger than the size of the emitting area. Although the exact emitter lengths are impossible to determine, we may still conclude that an effective exciton localization in the NW axial direction takes place in our structures.

## V. MAGNETO-OPTICAL STUDY

The most intriguing part about the thermally thinned NWs concerns the impact of NW size on the ground state character of the optical emission. It has been shown that in the most low-dimensional structures, as quantum dots or quantum wells, it usually exhibits HH character. This is caused by the shape anisotropy, i.e., small height compared to the lateral sizes of the nanostructures, as well as by the presence of the strain that is an inherent property of these structures. As a notable exception, the LH emission from quantum dots has been observed in specially designed heterostructures including a stressor layer [26] and in (Cd,Mn)Te/ZnTe NW quantum dot [27].

In the case of core/shell NWs built of zinc-blende semiconductors, the character of the emission is highly dependent on

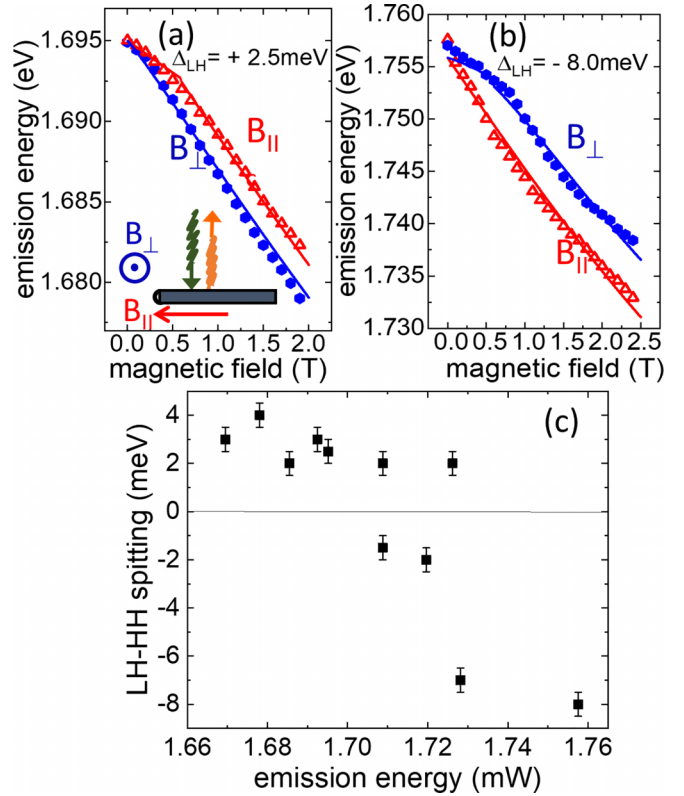


FIG. 4. (a), (b) Magnetic field dependence of the position of optical emission lines from two different NWs showing either light hole (LH) or heavy hole (HH) character. Magnetic field is applied either along, red triangles, or perpendicular, blue circles, to the NW axis in the geometry shown in the inset of (a). Solid lines represent fits which lead us to determine LH-HH splitting values  $\Delta_{LH}$ . The fitting procedure is described in the text. (c) LH-HH splitting plotted vs emission energy for ten different NWs. The emission from the most NWs emitting above 1.71 eV has HH character. LH character is typical for the NWs emitting below 1.71 eV. Temperature of the measurements is 7 K, excitation wavelength 532 nm (2.33 eV).

the strain between the core and the shell [28,29]. In the case of a tensile strain acting on the NW cores, the emission from the ground state has a HH character [20], while compressive strain leads to a predominantly LH character of the ground state [19]. In the case of NWs with wurtzite structure, such as in wurtzite CdTe/(Cd,Mg)Te core/shell NWs, the ground state usually has the HH character despite compressive strain acting on the NW core [24].

In order to explore the ground state character of the excitonic emission in our case, photoluminescence of individual NWs in an external magnetic field was measured, similarly to Refs. [19,20]. The field was applied either along or perpendicular to the NW axis in the geometry shown schematically in the inset of Fig. 4(a). The dependence of emission energy on magnetic field magnitude and direction is fitted within the frame of six band  $kp$  model calculations, including two LH and two HH bands, from which the magnitude and the sign of the LH-HH splitting  $\Delta_{LH}$  is determined [20]. The use of this model might be an oversimplification, since the proper description should involve the impact of excited states and the interaction of LH band with the spin-orbit split band [30]. We

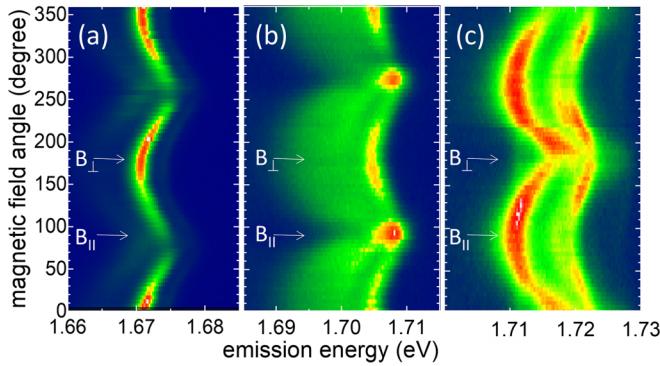


FIG. 5. Photoluminescence spectra from individual NWs as a function of magnetic field direction applied in the plane of the sample in Faraday configuration with  $|B| = 2$  T. The directions parallel and perpendicular to the NW axis are marked. (a) LH character of the emission  $\Delta_{\text{LH}} = 4$  meV. (b) LH character  $\Delta_{\text{LH}} = 2$  meV, Zeeman splitting is comparable to  $\Delta_{\text{LH}}$  value (c) HH character  $\Delta_{\text{LH}} = -7$  meV.

justify it, however, by relatively small strain values present in our system and quite deep valence band offset, which prevents the hole wave function to be significantly delocalized outside of the NW core. In these conditions, the use of the six band model should be well applicable [30]. For each NW selected for this experiment, the orientation of the NW axis in the laboratory frame has been determined thanks to the high linear polarization anisotropy of the optical emission [31]. The results for two NWs characterized by qualitatively different magnetic-field behavior are presented in Figs. 4(a) and 4(b). In Fig. 4(a), the magnetic field induced energy shift is larger in the perpendicular field configuration compared to the parallel field configuration, which is typical for a LH character of the optical emission. On the other hand, an opposite effect occurs in Fig. 4(b), evidencing a HH character of the excitons in this NW.  $\Delta_{\text{LH}}$  values are determined from the theoretical fits to the experimental data performed by applying the procedure described in [20] (solid lines in Fig. 4) and amount to +2.5 and  $-8$  meV for the NW considered in Figs. 4(a) and 4(b), respectively.

A similar procedure was carefully applied to a set of individual NWs, allowing us to capture a distinct relationship between the emission energy of the investigated NW and its ground state character, Fig. 4(c). NWs emitting lower energy were observed to display a LH ground state character, which transitions to a HH character with increasing emission energy. The transition between them, corresponding to a degenerate character of the ground state, occurs at roughly 1.71 eV. This is in good agreement with our previous results [19], where the ground state was observed to be of LH character for lower energies in not thinned (Cd,Mn)Te/(Cd,Mg)Te core/shell NWs.

The change of the ground state character is not only a quantitative measure: it is a qualitative change of behavior, which alters the properties of the emission. This is emphasized by the complementing measurements of photoluminescence in the magnetic field applied with a constant absolute value of 2 T as a function of the direction within the plane of the sample. Those results are presented in Fig. 5, where the emission energy is plotted as a function of the angle between

the NW axis and the magnetic field direction, with the color marking the intensity of the emission for three different NWs.

Figure 5(a) corresponds to a NW with LH character of the ground state, Fig. 5(b) to a NW with a nearly degenerate hole states, but still having the LH character at 0 T, and finally Fig. 5(c) to a NW with a distinct HH character. When comparing Fig. 5(a) to Fig. 5(c), one observes a qualitatively different behavior. The lowest emission energy, which corresponds to the largest energy shift, is observed when applying a magnetic field either perpendicular, Fig. 5(a), or parallel to the NW axis, Fig. 5(c), which is the defining characteristic of the corresponding ground state.

An additional, interesting pattern is presented in Fig. 5(b); a case of a NW in which the optical emission has a LH character at  $B = 0$  T, but  $\Delta_{\text{LH}}$  amounts to only 2 meV. For the parallel field configuration, a maximum in PL intensity is observed, which is not visible in the case of Fig. 5(a), even though it exhibits a LH character as well. This effect is most likely caused by the appearance of HH exciton, related emission, which is expected to exhibit a larger energy shift compared to LH excitons at the magnetic field applied parallel to the NW axis. In this configuration, as a result of a small  $\Delta_{\text{LH}}$  value, it is possible that LH and HH exciton energies become comparable to each other, leading to the appearance of HH-related emission. When the magnetic field direction is changed, the difference between the two lowest-lying states increases rapidly, resulting in the presence of only one optical transition.

We also note the presence of a second emission line in Fig. 5(c), dedicated to studying of magnetic field direction dependence of the emission with predominantly HH character. This line appears at a higher energy and exhibits similar behavior to the brighter line. We conclude, therefore, that it is also associated to the HH recombination but with electrons with an opposite spin, i.e., to the recombination of dark excitons. This interpretation is consistent with the fact that the intensity of the second line is the lowest for the parallel magnetic field, when the dark exciton recombination is forbidden by the optical selection rules, and that it increases distinctly when a perpendicular field component appears.

## VI. DISCUSSION

The change from LH to HH character of the excitonic emission in our structures as a function of the emission energy is, most likely, a consequence of the exciton localization due to NW-core diameter variation. NW-core diameter variation implies that the ground state exciton energy changes as a function of its axial position. In this situation, the excitons localize at the lowest energy areas and may be trapped inside the so-called natural NW quantum dots, which represent zero-dimensional traps for electrons and holes. This effect would also be consistent with CL measurements which indicate the presence of exciton localization areas along the NW axis. Up to date, NW quantum dots have been fabricated by inserting a low band-gap NW segment axially into the large band-gap NW core. These structures have been intensively studied due to the single photon character of the optical emission [23,32–34]. As predicted theoretically, the LH/HH character of the ground state in these structures may exhibit a change depend-

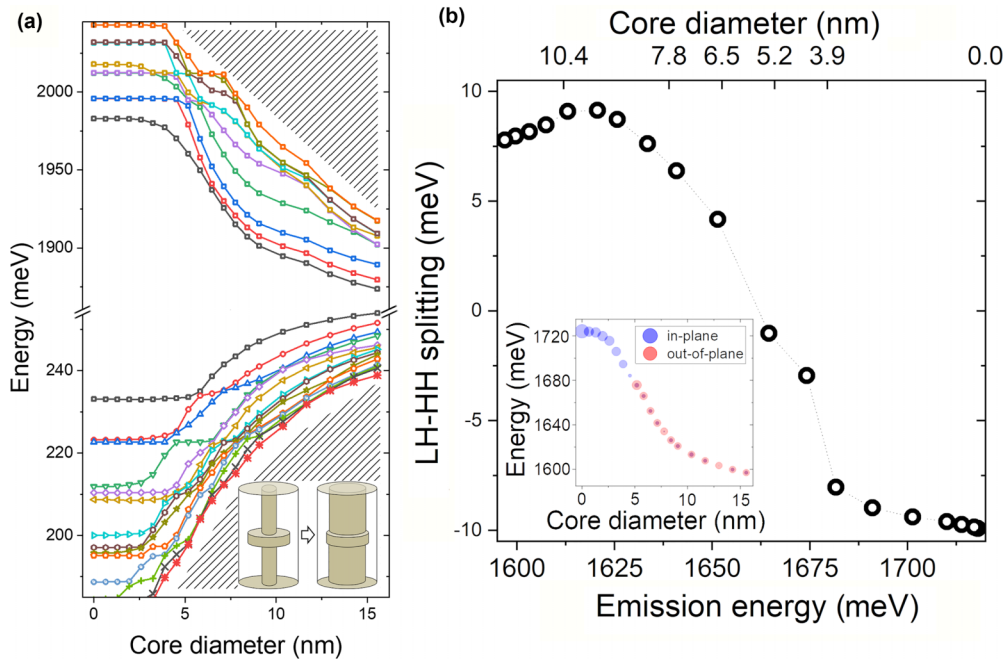


FIG. 6. Results of atomistic calculations as a function of core thickness for (a) single-particle electron and hole energies, (b) light-hole/heavy-hole splitting with bottom  $x$  axis representing emission energy and top corresponding to core diameter. Inset in (b) presents excitonic ground state energy dependence on core diameter with diameters of circles proportional to excitonic optical activity and colors describing the polarization of emitted light. Inset in (a) shows schematically the increase of core thickness. At approximately 6 nm core thickness there is a crossing from a heavy-hole to a light-hole ground state reflected both in the single particle and many-body spectra.

ing on the length of this low band-gap segment [35]. This effect could also explain the fact that the (Cd,Mn)Te quantum dot within ZnTe NW may exhibit either LH [27] or HH character [20] depending on the report. Recently performed theoretical considerations of strained (Cd,Mn)Te/ZnTe ellipsoidal quantum dots confirm that the valence band ground state in these structures may depend on the size of CdMnTe quantum dot [30]. These results lead us to assume that in the case of natural NW quantum dots studied in this work the experimentally observed change from LH to HH character of the ground state could just as likely be explained by different sizes of the emitting structures.

In CdTe/(Cd,Mg)Te core/shell NWs with core diameters larger than 20 nm the excitonic emission has been demonstrated to exhibit LH character due to compressive strain acting on the NW core and  $\Delta_{\text{LH}}$  values in the range 7–15 meV [19]. Atomistic modeling demonstrates that solely a strong localization of excitons along the NW axis may induce the experimentally observed change from LH to HH character of the valence band maximum.

Comparison of experimental results with theory, however, is always challenging due to uncertainty of size, shape, and the actual chemical composition. Modeling (Cd,Mg)Te systems is complicated further since  $\text{Cd}_{1-x}\text{Mg}_x\text{Te}$  alloy is still under active research, with many bulk properties determined with significant uncertainties. Nonetheless, the experimental findings were augmented by theoretical modeling, which allowed us to capture the underlying effects leading to the observed phenomena.

The procedure of atomistic modeling starts with finding atomic positions that minimize total elastic energy using Keat-

ing's valence force field method [36,37] and minimization of strain energy performed with the conjugate gradient method [38]. For CdTe, we take parameters from [36]; for MgTe we use parameters described in our earlier work [39]. Since we do not have a set of valence force field (VFF) parameters for  $\text{Cd}_{1-x}\text{Mg}_x\text{Te}$  alloy, we determine them in the spirit of virtual crystal approximation by combining CdTe and MgTe parameters and assuming  $x = 0.35$ , consistent with experimental findings. Once atomic positions are found, we obtain a single-particle electron and hole states with the empirical tight-binding  $sp^3s^*$  approach accounting for spin-orbit interaction [40] and strain via the Harrison scaling law of hopping matrix elements [41].

For CdTe tight-binding model, we used a set of empirical tight-binding parameters for  $\text{Cd}_{1-x}\text{Mg}_x\text{Te}$  alloy [42]; we developed a set of parameters starting to form pure CdTe, and the shifting material band gap, via a shift of on-site (diagonal) energies of  $s$  orbitals, and additionally by accounting for a valence-band offset between core and shell materials [43]. Next, the excitonic spectra are calculated using the configuration-interaction method described in Refs. [44,45] with Coulomb and dipole matrix elements calculated using an approach presented in Refs. [44,46].

A system reproducing at least qualitatively the experimental data is found to be a quantum dot of a constant size embedded in a NW of a varying diameter, inset in Fig. 6(a). It is worth noticing that a similar feature is visible on the SEM image in Fig. 1(b). Figures 6(a) and 6(b) show the evolution of single-particle energies as a function of CdTe core diameter. Here, the core diameter is increased from 0 to 15.5 nm with fixed dimensions of the CdTe section (height of 2.25 nm



and diameter of 19.4 nm). The QD has a substantially larger diameter than the core itself, representing a “bulge” shown on the inset in Fig. 6(a).

Both core and large diameter CdTe sections are embedded into  $\text{Cd}_{0.65}\text{Mg}_{0.35}\text{Te}$  NW with a fixed shell diameter equal to 32.4 nm and a total length (along the growth direction) of 45 nm. For a case with a core diameter equal to zero (i.e., no core), the spectra of the system naturally correspond to spectra of a single quantum dot with clearly apparent shell structure of electron and hole states. With an increasing core diameter, these states undergo a pronounced evolution that removes the shell structure of a quasi-zero-dimensional system, with electron (hole) levels experiencing a strong redshift (blueshift) due to reduced confinement in the growth direction. With increasing core diameter, at approximately 6 nm, the ground hole state of a HH character crosses with a LH state, which then becomes the hole ground state. This crossing results from reduced and reversed LH/HH splitting coming from increasing core diameter [Fig. 6(b) and is reflected in the excitonic spectra as well. As shown in inset in Fig. 6(b), the ground excitonic energy evolution reflects the reduction of confinement shown in electron and hole spectra.

Thus, what we observe is an evolution from a dotlike system to a dot-in-a-NW system with a wider section spectra strongly hybridized with the NW core. Additionally, the change of the ground hole state character is reflected in the excitonic spectra [29] by a change of the dominant polarization direction of emitted light, from in-plane (“ $x$ ,  $y$ ”) to out-of-plane (“ $z$ ”) direction. However, we must not forget that the polarization of light measured experimentally may strongly depend on the polarization properties of a host NW [47], which impedes the direct experimental determination of the emission polarization given solely by the optical selection rules.

In summary, we have successfully grown (Cd,Mn)Te/(Cd,Mg)Te core/shell NWs, in which NW cores reach diameters below 10 nm. The thinning procedure relies on thermal treatment of NW cores, which takes place before the shell deposition. The optical emission from these structures reveals multiple signs of quantum confinement effects. The emission energy exhibits a considerable blueshift compared to the reference sample, which was not subject to the thermal treatment. Moreover, excited states related emission and multiexcitonic complexes such as biexcitons are observed in the emission spectra from individual NWs. Interestingly, cathodoluminescence measurements reveal that the optical emission originates from only a certain part of the NW, which implies that carrier localization takes place not only in radial, but also in the axial direction of the NW. Finally, a detailed magneto-optical study reveals that the ground state character exhibits a clear dependence on the emission energy as well. Majority of NWs emitting below 1.71 eV exhibits a LH character, whereas a HH character is typical for the NWs emitting in higher energy. The observed effects are explained in terms of the presence of additional axial carrier confinement induced by fluctuations of the core diameter. Theoretical considerations, using the atomistic tight-binding approach, demonstrate that the axial quantum confinement can be the source of the ground state character transition.

#### ACKNOWLEDGMENT

This work has been partially supported by the National Centre of Science (Poland) through Grant No. 2017/26/E/ST3/00253.

The authors have no conflicts to disclose. Data are available on request from the authors.

- 
- [1] M. Fox and R. Ispasoiu, in *Quantum Wells, Superlattices, and Band-Gap Engineering, in Quantum Wells, Superlattices, and Band-Gap Engineering, Springer Handbooks* (Springer, New York, 2007), pp. 1021–1040.
  - [2] A. M. Morales and C. M. Lieber, A laser ablation method for the synthesis of crystalline semiconductor nanowires, *Science* **279**, 208 (1998).
  - [3] R. S. Wagner and W. C. Ellis, Vapor-liquid-solid mechanism of single crystal growth, *Appl. Phys. Lett.* **4**, 89 (1964).
  - [4] E. Kapon, D. M. Hwang, and R. Bhat, Stimulated Emission in Semiconductor Quantum Wire Heterostructures, *Phys. Rev. Lett.* **63**, 430 (1989).
  - [5] H. S. Yeo, K. Lee, Y. C. Sim, S. H. Park, and Y. H. Cho, Strong and robust polarization anisotropy of site- and size-controlled single InGaN/GaN quantum wires, *Sci. Rep.* **10**, 1 (2020).
  - [6] S. Fust, A. Faustmann, D. J. Carrad, J. Bissinger, B. Loitsch, M. Döblinger, J. Becker, G. Abstreiter, J. J. Finley, and G. Koblmüller, Quantum-Confinement-Enhanced thermoelectric properties in Modulation-Doped GaAs–AlGaAs Core–Shell nanowires, *Adv. Mater.* **32**, 1905458 (2020).
  - [7] F. Dirnberger, M. Kammermeier, J. König, M. Forsch, P. E. Faria Jr., T. Campos, J. Fabian, J. Schliemann, C. Schüller, T. Korn *et al.*, Ultralong spin lifetimes in one-dimensional semiconductor nanowires, *Appl. Phys. Lett.* **114**, 202101 (2019).
  - [8] Y. Ducommun, E. Martinet, H. Weman, G. Biasiol, A. Gustafsson, and E. Kapon, Structure and optical properties of V-Groove quantum wire superlattices, *Physica E (Amsterdam, Neth.)* **2**, 954 (1998).
  - [9] H. Yu, J. Li, R. A. Loomis, L. W. Wang, and W. E. Buhro, Two-versus three-dimensional quantum confinement in indium phosphide wires and dots, *Nat. Mater.* **2**, 517 (2003).
  - [10] F. Wang, A. Dong, J. Sun, R. Tang, H. Yu, and W. E. Buhro, Solution-liquid-solid growth of semiconductor nanowires, *Inorg. Chem.* **45**, 7511 (2006).
  - [11] J. D. Holmes, K. P. Johnston, R. C. Doty, and B. A. Korgel, Control of thickness and orientation of solution-grown silicon nanowires, *Science* **287**, 1471 (2000).
  - [12] H. A. Fonseka, A. V. Velichko, Y. Zhang, J. A. Gott, G. D. Davis, R. Beanland, H. Liu, D. J. Mowbray, and A. M. Sanchez, Self-Formed quantum wires and dots in GaAsP–GaAsP Core–Shell nanowires, *Nano Lett.* **19**, 4158 (2019).

- [13] P. Corfdir *et al.*, Crystal-phase quantum wires: One-dimensional heterostructures with atomically flat interfaces, *Nano Lett.* **18**, 247 (2018).
- [14] B. Loitsch *et al.*, Tunable quantum confinement in ultrathin, optically active semiconductor nanowires via reverse-reaction growth, *Adv. Mater.* **27**, 2195 (2015).
- [15] J. K. Zettler *et al.*, Observation of dielectrically confined excitons in ultrathin GaN nanowires up to room temperature, *Nano Lett.* **16**, 973 (2016).
- [16] N. Vainorius, S. Lehmann, A. Gustafsson, L. Samuelson, K. A. Dick, and M. E. Pistol, Wurtzite GaAs quantum wires: One-dimensional subband formation, *Nano Lett.* **16**, 2774 (2016).
- [17] F. Del Giudice, J. Becker, C. De Rose, M. Döblinger, D. Ruhstorfer, L. Suomenniemi, J. Treu, H. Riedl, J. J. Finley, and G. Koblmüller, Ultrathin catalyst-free InAs nanowires on silicon with distinct 1D sub-band transport properties, *Nanoscale* **12**, 21857 (2020).
- [18] I. Ilkiv, D. Kirilenko, K. Kotlyar, and A. Bouravleuv, Thermal decomposition of GaAs nanowires, *Nanotechnology* **31**, 055701 (2020).
- [19] J. Płachta *et al.*, Magnetic field induced mixing of light hole excitonic states in (Cd, Mn)Te/(Cd, Mg)Te Core/Shell nanowires, *Nanotechnology* **29**, 205205 (2018).
- [20] M. Szymura *et al.*, Spin splitting anisotropy in single diluted magnetic nanowire heterostructures, *Nano Lett.* **15**, 1972 (2015).
- [21] P. Wojnar *et al.*, Growth and optical investigations of high quality individual CdTe/(Cd,Mg)Te Core/Shell Nanowires, *Nanotechnology* **28**, 045207 (2017).
- [22] Y. Z. Hu, S. W. Koch, M. Lindberg, N. Peyghambarian, E. L. Pollock, and F. F. Abraham, Biexcitons in Semiconductor Quantum Dots, *Phys. Rev. Lett.* **64**, 1805 (1990).
- [23] M. E. Reimer, G. Bulgarini, N. Akopian, M. Hocevar, M. B. Bavinck, M. A. Verheijen, E. P. A. M. Bakkers, L. P. Kouwenhoven, and V. Zwiller, Bright single-photon sources in bottom-up tailored nanowires, *Nat. Commun.* **3**, 1 (2012).
- [24] J. Płachta, A. Kaleta, S. Kret, T. Kazimierczuk, K. Połczyńska, P. Kossacki, G. Karczewski, T. Wojtowicz, J. Kossut, and P. Wojnar, Polarization and magneto-optical properties of excitonic emission from wurtzite CdTe/(Cd,Mg)Te Core/Shell nanowires, *Nanotechnology* **31**, 215710 (2020).
- [25] A. Gustafsson, J. Bolinsson, N. Sköld, and L. Samuelson, Determination of diffusion lengths in nanowires using cathodoluminescence, *Appl. Phys. Lett.* **97**, 072114 (2010).
- [26] Y. H. Huo *et al.*, A light-hole exciton in a quantum dot, *Nat. Phys.* **10**, 46 (2013).
- [27] M. Jeannin, A. Artioli, P. Rueda-Fonseca, E. Bellet-Amalric, K. Kheng, R. André, S. Tatarenko, J. Cibert, D. Ferrand, and G. Nogues, Light-hole exciton in a nanowire quantum dot, *Phys. Rev. B* **95**, 035305 (2017).
- [28] A. Artioli *et al.*, Optical properties of single ZnTe nanowires grown at low temperature, *Appl. Phys. Lett.* **103**, 222106 (2013).
- [29] D. Ferrand and J. Cibert, Strain in crystalline core-shell nanowires, *Eur. Phys. J.: Appl. Phys.* **67**, 30403 (2014).
- [30] K. Moratis, J. Cibert, D. Ferrand, and Y. M. Niquet, Light hole states in a strained quantum dot: Numerical calculation and phenomenological models, *Phys. Rev. B* **103**, 245304 (2021).
- [31] J. Wang, M. S. Gudiksen, X. Duan, Y. Cui, and C. M. Lieber, Highly polarized photoluminescence and photodetection from single indium phosphide nanowires, *Science* **293**, 1455 (2001).
- [32] S. Bounouar *et al.*, Ultrafast room temperature single-photon source from nanowire-quantum dots, *Nano Lett.* **12**, 2977 (2012).
- [33] M. T. Borgström, V. Zwiller, E. Müller, and A. Imamoglu, Optically bright quantum dots in single nanowires, *Nano Lett.* **5**, 1439 (2005).
- [34] P. Wojnar, E. Janik, L. T. Baczewski, S. Kret, G. Karczewski, T. Wojtowicz, M. Goryca, T. Kazimierczuk, and P. Kossacki, Growth and optical properties of CdTe quantum dots in ZnTe nanowires, *Appl. Phys. Lett.* **99**, 113109 (2011).
- [35] M. Zieliński, Fine structure of light-hole excitons in nanowire quantum dots, *Phys. Rev. B* **88**, 115424 (2013).
- [36] R. M. Martin, Elastic properties of ZnS structure semiconductors, *Phys. Rev. B* **1**, 4005 (1970).
- [37] P. N. Keating, Effect of invariance requirements on the elastic strain energy of crystals with application to the diamond structure, *Phys. Rev.* **145**, 637 (1966).
- [38] W. Jaskólski, M. Zieliński, G. W. Bryant, and J. Aizpurua, Strain effects on the electronic structure of strongly coupled self-assembled InAs/GaAs quantum dots: Tight-binding approach, *Phys. Rev. B* **74**, 195339 (2006).
- [39] P. Wojnar *et al.*, Strain-Induced energy gap variation in ZnTe/ZnMgTe Core/Shell nanowires, *Appl. Phys. Lett.* **104**, 163111 (2014).
- [40] D. J. Chadi, Spin-orbit splitting in crystalline and compositionally disordered semiconductors, *Phys. Rev. B* **16**, 790 (1977).
- [41] W. A. Harrison, *Electronic Structure and the Properties of Solids: The Physics of the Chemical Bond* (Dover, New York, 1989).
- [42] A. Kobayashi, O. F. Sankey, and J. D. Dow, Chemical trends for defect energy levels in  $\text{Hg}_{(1-x)}\text{Cd}_x\text{Te}$ , *Phys. Rev. B* **25**, 6367 (1982).
- [43] J. H. Yang, S. Chen, W. J. Yin, X. G. Gong, A. Walsh, and S. H. Wei, Electronic structure and phase stability of MgTe, ZnTe, CdTe, and their alloys in the B3, B4, and B8 structures, *Phys. Rev. B* **79**, 245202 (2009).
- [44] M. Zieliński, M. Korkusiński, and P. Hawrylak, Atomistic tight-binding theory of multiexciton complexes in a self-assembled InAs quantum dot, *Phys. Rev. B* **81**, 085301 (2010).
- [45] P. T. Rózański and M. Zieliński, Efficient computation of coulomb and exchange integrals for multi-million atom nanostructures, *Comput. Phys. Commun.* **238**, 254 (2019).
- [46] S. Schulz, S. Schumacher, and G. Czycholl, Tight-binding model for semiconductor quantum dots with a wurtzite crystal structure: From one-particle properties to coulomb correlations and optical spectra, *Phys. Rev. B* **73**, 245327 (2006).
- [47] D. Van Dam, D. R. Abujetas, R. Paniagua-Domínguez, J. A. Sánchez-Gil, E. P. A. M. Bakkers, J. E. M. Haverkort, and J. Gómez Rivas, Directional and polarized emission from nanowire arrays, *Nano Lett.* **15**, 4557 (2015).